Science Advances
AAAS

advances.sciencemag.org/cgi/content/full/6/41/eabc9846/DC1

Supplementary Materials for

3D printed self-supporting elastomeric structures for multifunctional microfluidics

Ruitao Su, Jiaxuan Wen, Qun Su, Michael S. Wiederoder, Steven J. Koester, Joshua R. Uzarski, Michael C. McAlpine*

*Corresponding author. Email: mcalpine@umn.edu

Published 9 October 2020, *Sci. Adv.* **6**, eabc9846 (2020)
DOI: 10.1126/sciadv.abc9846

The PDF file includes:

Other Supplementary Material for this manuscript includes the following:

(available at advances.sciencemag.org/cgi/content/full/6/41/eabc9846/DC1)

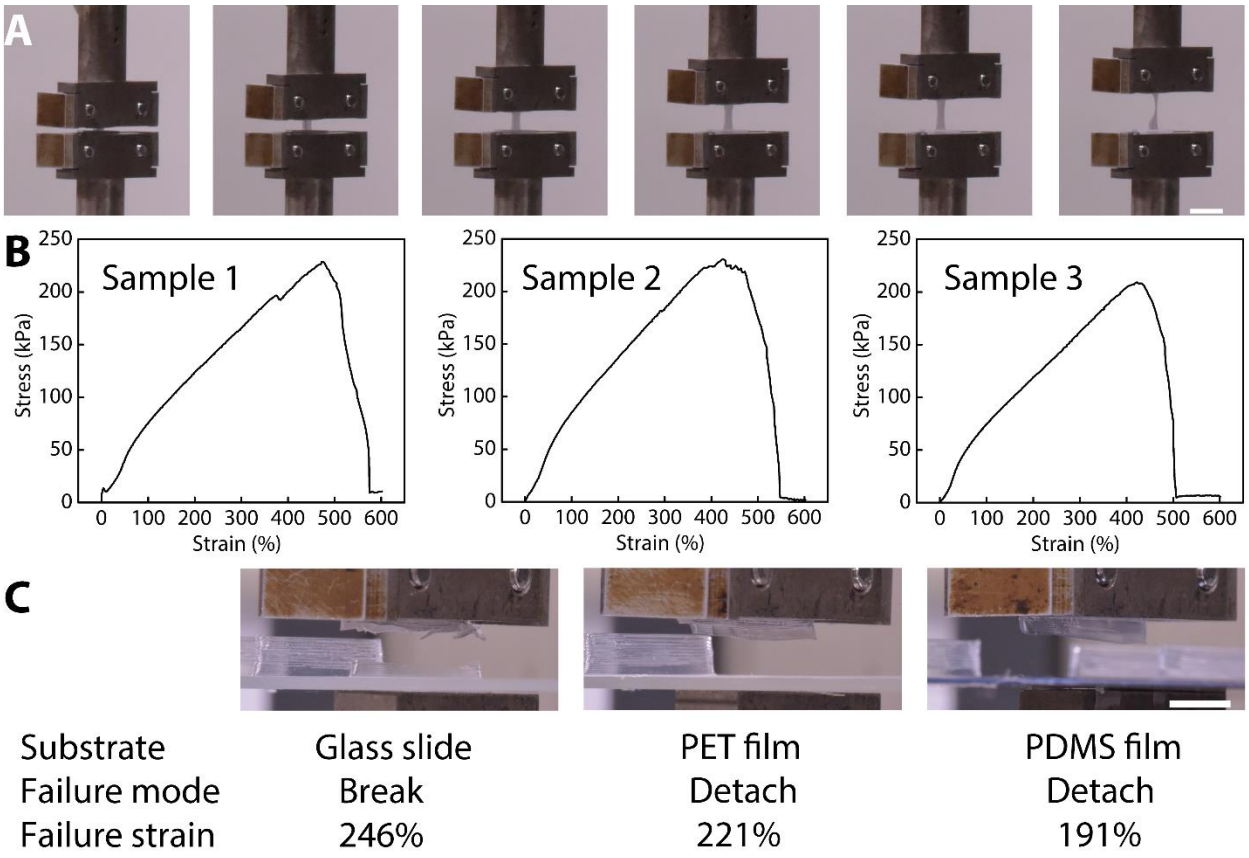

Fig. S1. Elongation and adhesion tests of cured silicone walls. (**A**) Images of elongation test along the printing direction of a cured silicone wall. The tested samples are 0.3 mm (thickness) × 3.5 mm (width) × 1.5 mm (initial gap). (**B**) Strain-stress curves of cured silicone walls. (**C**) Adhesion tests of cured silicone walls printed onto three different substrates. Pulling direction is perpendicular to the printing direction. PET film was attached to a glass slide. PDMS film was spin-coated onto a silicon wafer. Scale bars are 5 mm. Photo credit: Ruitao Su, University of Minnesota.

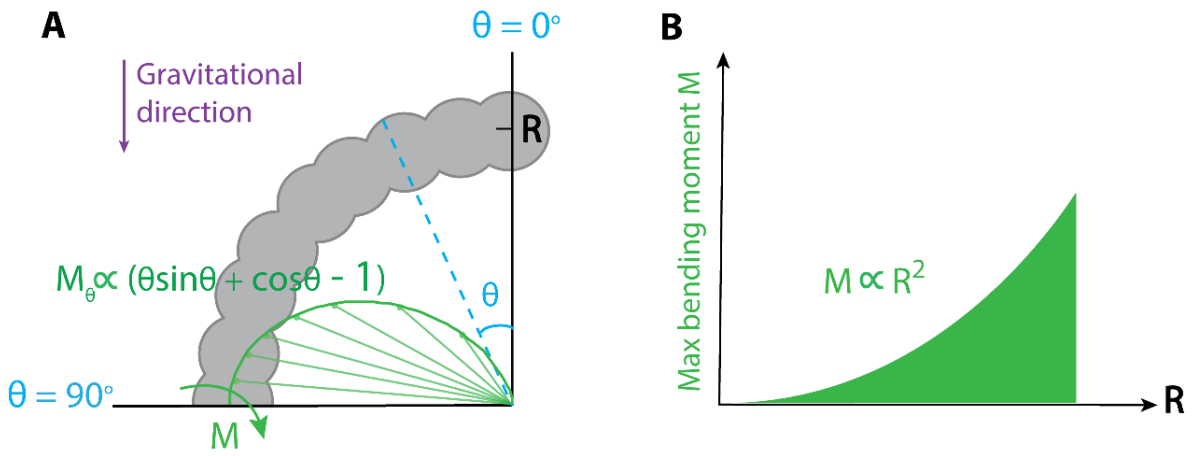

Fig. S2. Bending moment analysis of silicone walls printed with circular profiles. (**A**) Bending moment distribution along a self-supporting wall. (**B**) The maximum bending moment increases parabolically with the radius of the wall.

Analysis of the bending moment for the 3D printed circular silicone wall:

$$M_\theta = R^2\gamma(\theta \sin\theta + \cos\theta - 1) \quad (1)$$

$$M = \left(\frac{\pi}{2} - 1\right) R^2\gamma \quad (2)$$

where M_θ is the bending moment on the cross-section at the angular location θ, γ is the linear specific weight of the silicone wall, R is the radius of the circular wall, and M is the maximum bending moment at the root of the wall. As illustrated in fig. S2, the bending moment along the silicone wall increases in the direction towards the substrate, reaching the maximum value at the root of the wall. The maximum bending moment increases parabolically with the radius R. For the printed circular samples with channel widths below 1 mm ($R \leq 500$ µm), the yield strength of the RTV silicone walls can withstand the maximum bending moment induced by gravitational loading without any observed deformation.

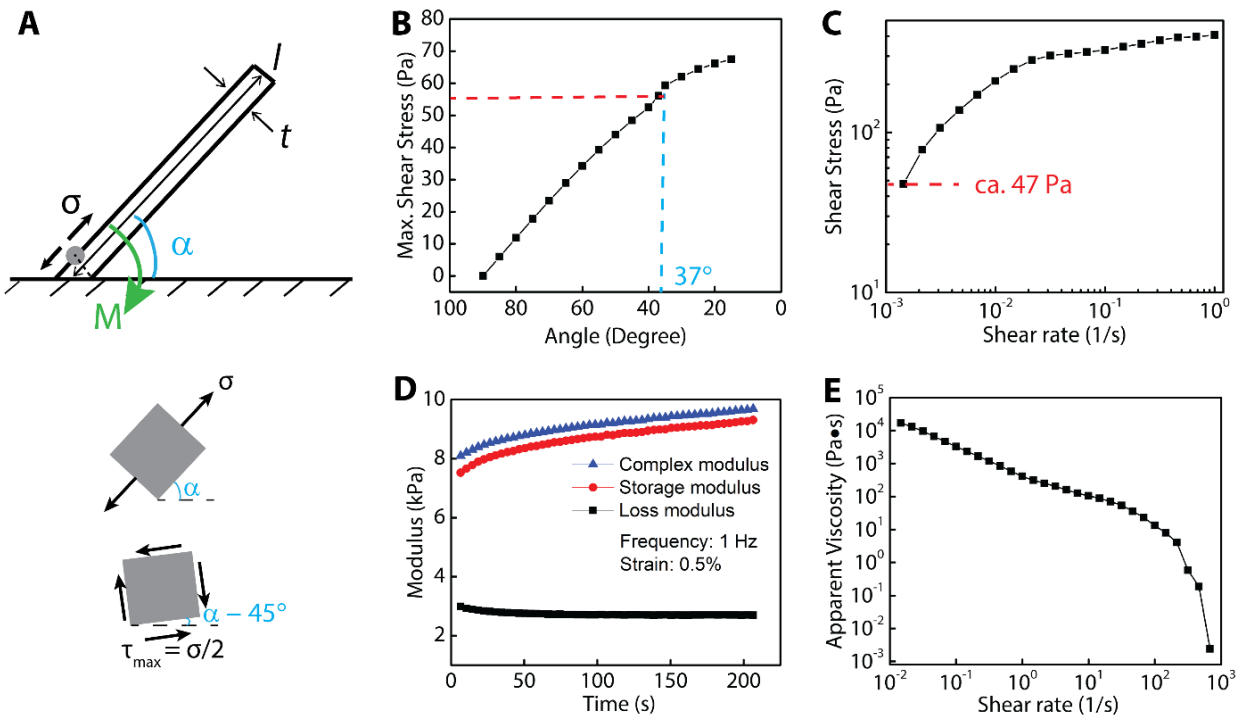

Fig. S3. Stress state analysis of silicone walls and rheology tests of uncured RTV silicone. (**A**) Diagram of stress state at the wall root. (**B**) Plot of predicted maximum shear stress at the wall root. (**C**) Flow sweep of uncured RTV silicone showed a yield stress of ca. 47 Pa, which increases as the material continuously cures in air. (**D**) Storage modulus increases as RTV silicone cures in air. (**E**) Apparent viscosity of RTV silicone decreases with shear rate.

Stress state analysis (Maximum shear stress criterion):

$$I_c = \frac{b(t)^3}{12} \tag{3}$$

$$\sigma = \frac{Mt}{2I_c} = \frac{3\rho g l^2}{t}\cos\alpha \tag{4}$$

$$\tau_{max} = \frac{\sigma}{2} \tag{5}$$

where I_c is the centroidal moment of inertia of the inspected cross-section (denoted by the dash line), b is the width of wall segment under inspection, t is the thickness of the silicone wall, σ is

principal stress of the inspected point (denoted by the end dot), ρ is the density of the uncured RTV silicone, g is the gravitational acceleration, l is the length of the silicone wall and τ_{max} is the maximum shear stress. The inspected silicone wall has an average thickness of 110 μm and length of 700 μm. The uncured RTV silicone has a density of 1.008 g/cm^3.

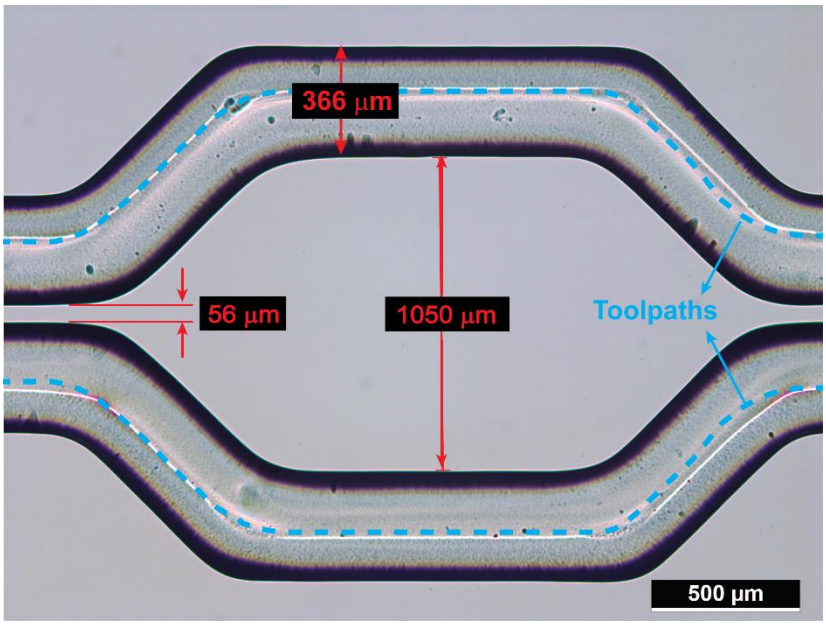

Fig. S4. Printing different channel widths with a 100 µm nozzle. The diameter of printed silicone filaments was offset in the design of the printing toolpaths to achieve the desired channel width. Photo credit: Ruitao Su, University of Minnesota.

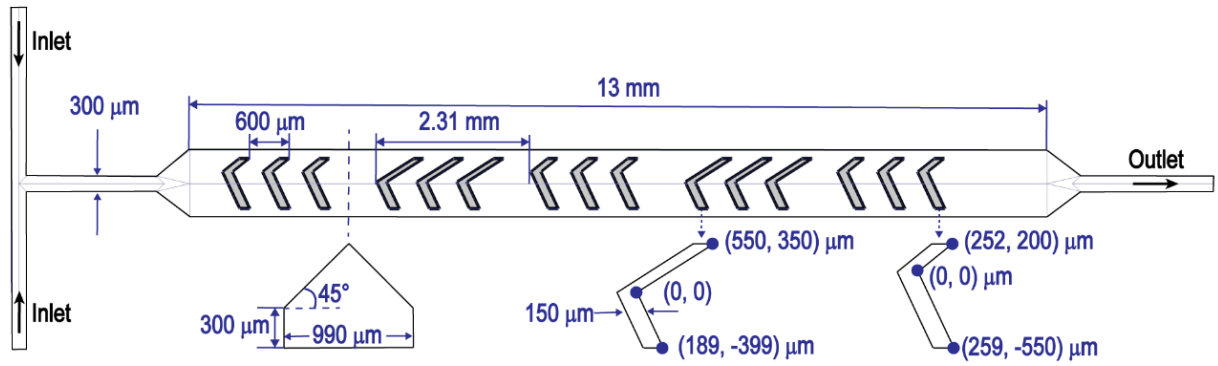

Fig. S5. Design of microfluidic mixers. Geometry and layout of the 3D printed multi-material microfluidic mixers integrated with herringbone ridges.

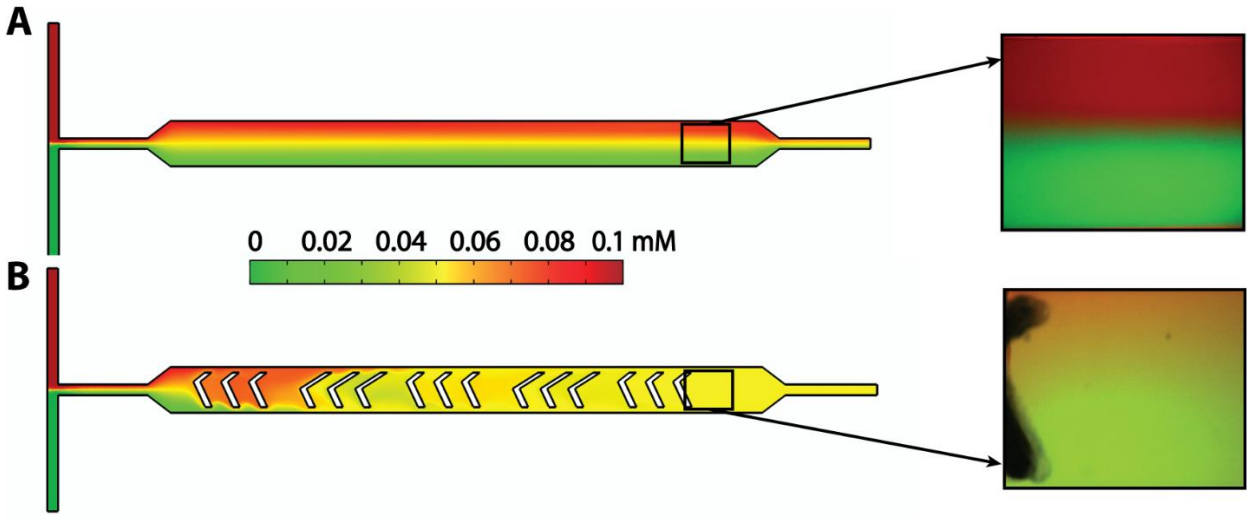

Fig. S6. Comparison between simulation and confocal microscopic images at the outlet. The simulated color map of the mixing profile taken on a plane 10 μm above the substrate and corresponding confocal microscope images at the outlet for (**A**) blank and (**B**) 350 μm HB ridge-embedded mixing channels. Re = 1. Photo credit: Ruitao Su, University of Minnesota.

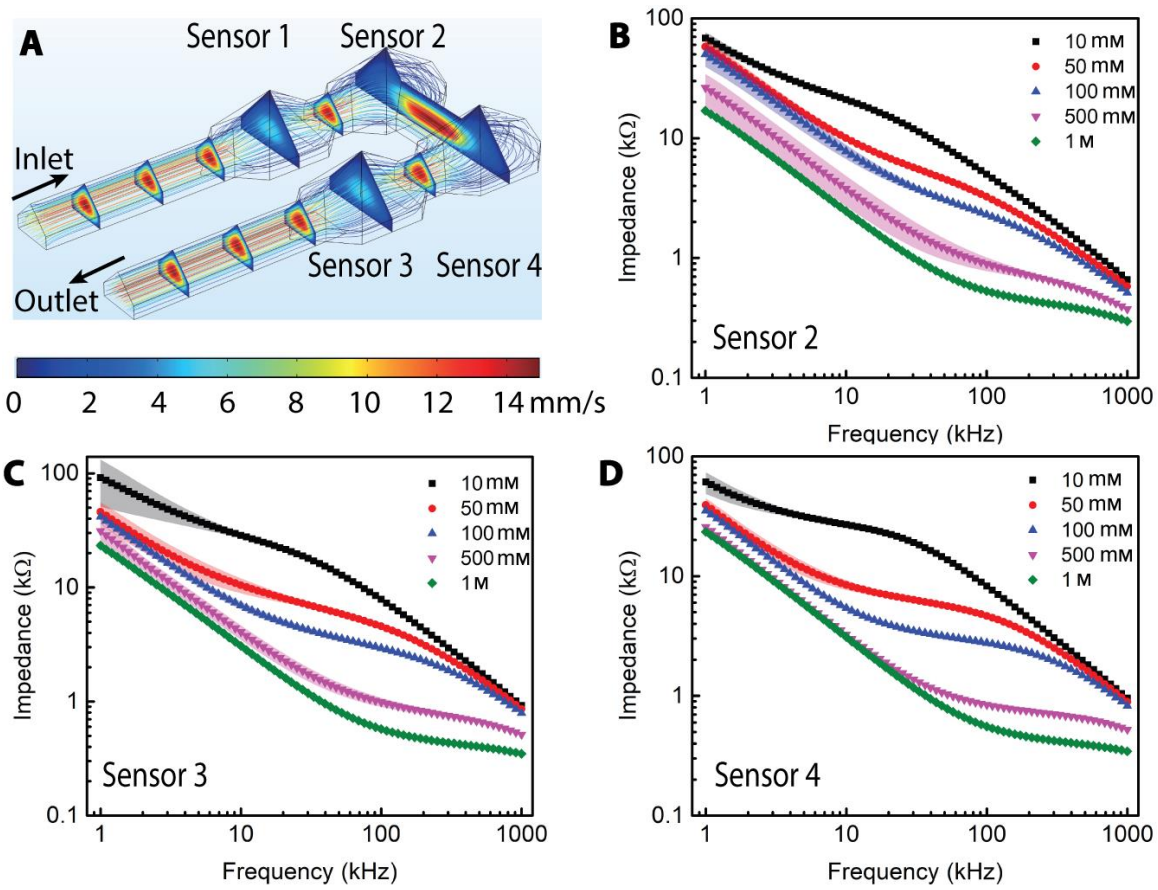

Fig. S7. Impedance spectra of Sensors 2-4. (**A**) CFD simulation showing highly laminar flow within the salinity sensor. (**B-D**) Impedance spectra measured with Sensors 2-4 of the 3D printed salinity sensing array for NaCl solutions of varying concentrations.

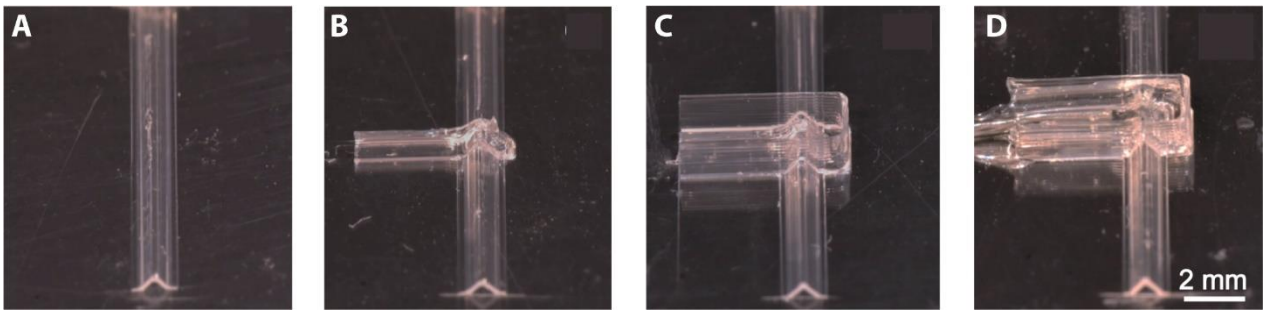

Fig. S8. Steps for printing the microfluidic valve. (**A**) Print the flow channel. (**B**) Print the overlapping control channel. (**C**) Print the container for the encapsulation material. (**D**) Insert connection tubing into the control channel, fill the container with UV-curable polymer and cure with 400 nm UV light. Photo credit: Ruitao Su, University of Minnesota.

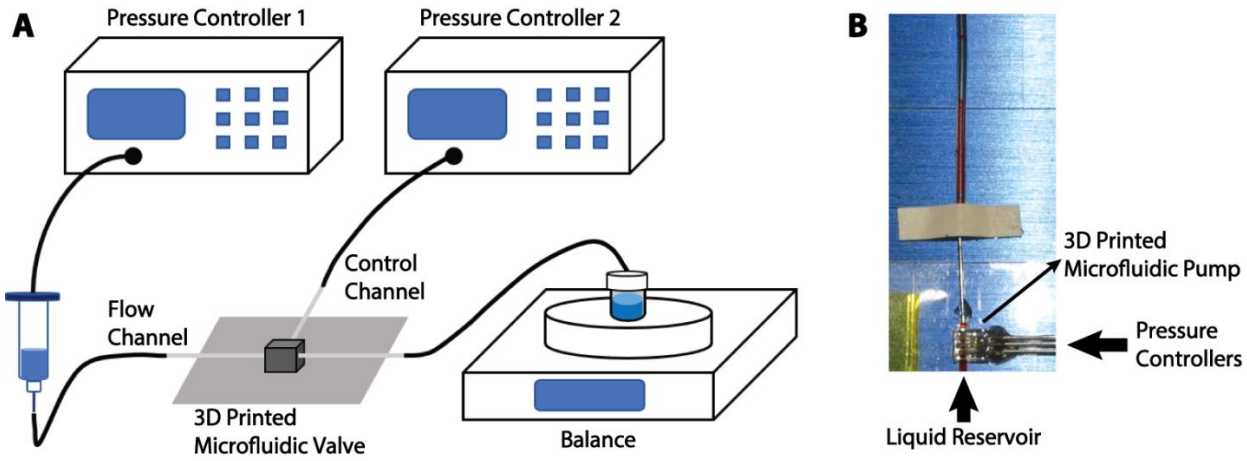

Fig. S9. Test setups for microfluidic valves and pumps. (**A**) Setup scheme for the valve closing tests, in which a balance was used to measure the quantity of water that flowed through the valve. (**B**) Setup scheme for the pump rate tests, where videos were taken to track the distance traveled by the fluid in the transparent tubing. Photo credit: Ruitao Su, University of Minnesota.

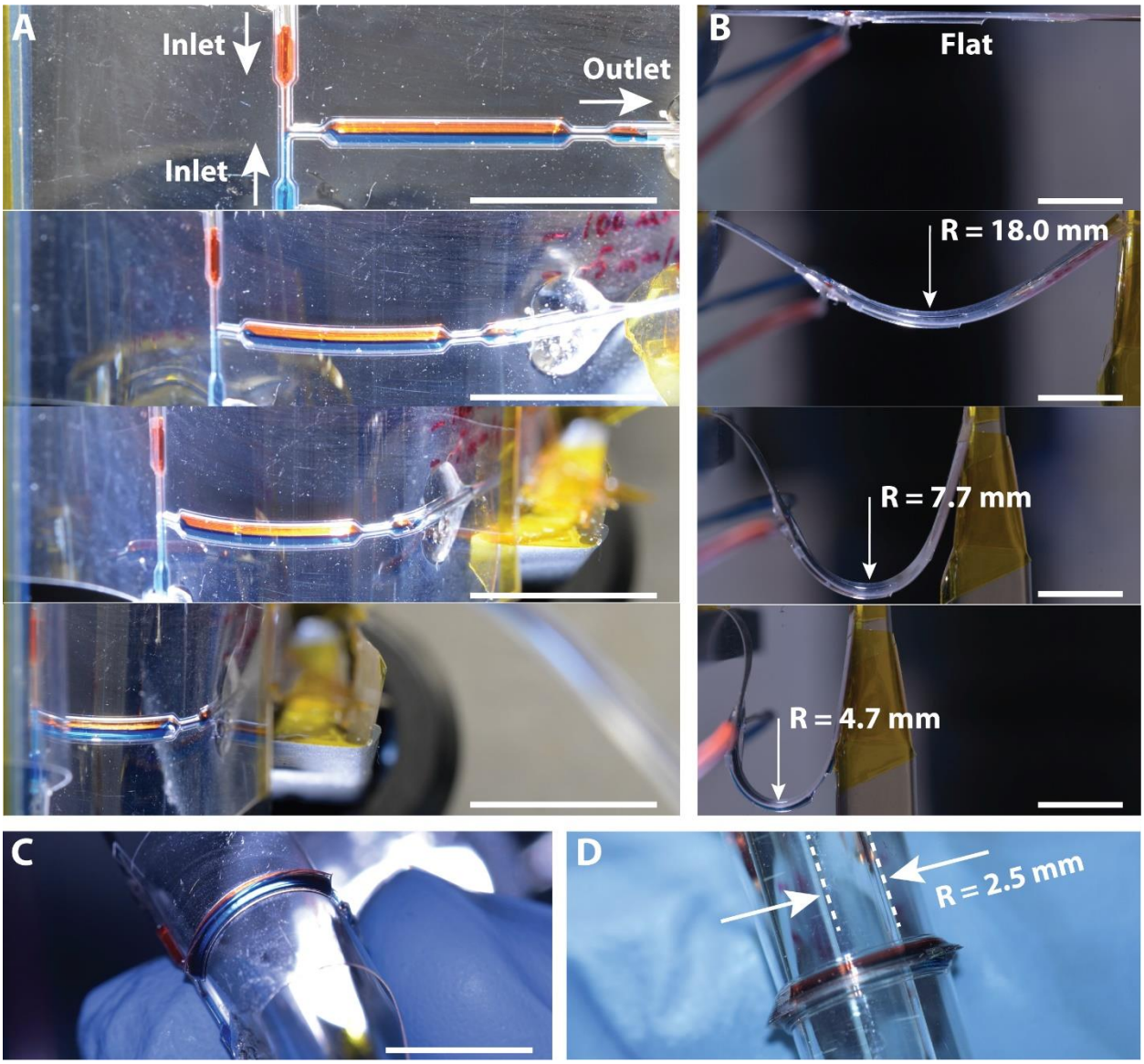

Fig. S10. Bending tests of a 3D printed two-inlet microfluidic channel on a PET film. All tests were done with a flow rate of 50 µL/min. (**A** & **B**) Top and side views of the channel bent with different radii of curvature. (**C**) Manually bent microfluidic channel. (**D**) The channel was wrapped onto a glass rod with a radius of 2.5 mm. Scale bars are 10 mm. Photo credit: Ruitao Su, University of Minnesota.

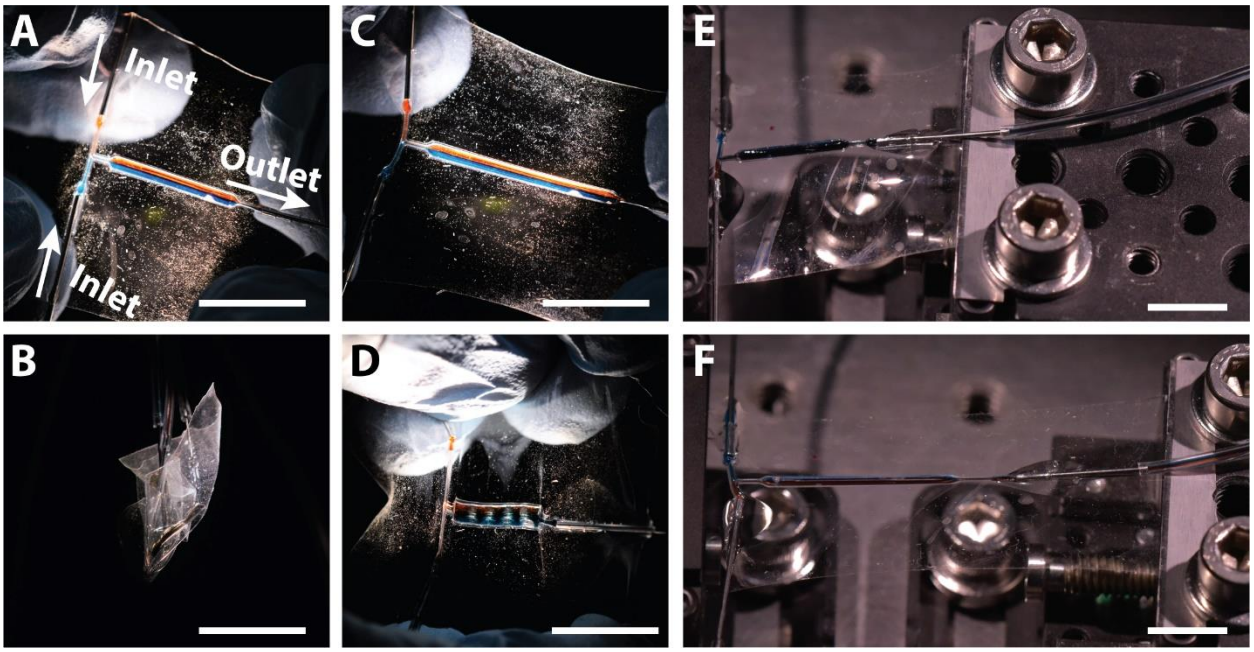

Fig. S11. Stretching tests of microfluidic channels printed on PDMS (Sylgard 184) films. All tests were done at a flow rate of 50 µm/min. (**A**) Hand-held microfluidic channel with two inlets. (**B**) Folded state of the channel-substrate assembly. (**C**) Manual stretch in the flow direction by ca. 40%. (**D**) Manual stretch in the transverse direction by ca. 85%. (**E**) Undeformed channel mounted on a translation stage. (**F**) The channel was stretched by 100%. Scales bars are 10 mm. Photo credit: Ruitao Su, University of Minnesota.

Table S1. Printing conditions for the self-supporting microfluidic structures

Device Type	**Nozzle Type**	**Nozzle Inner Diameter (μm)**	**Pressure (psi)**	**Speed (mm/s)**	**Distance to Substrate (μm)**	**Toolpath Resolution (μm)**	**Interlayer Distance (μm)**
Planar	Stainless steel	100	175	5	100	Continuous	70
Spherical	Tapered polypropylene	200	25	3	200	20 (valves) 50 (channels)	120